Bidimensional H-Bond Network Promotes Structural Order and Electron Transport in BPyMPMs Molecular Semiconductor : A Computational Study

Antonio de Nicola, Andrea Correa, Andrea Giunchi, Luca Muccioli, Gabriele d'Avino, Junji Kido, Giuseppe Milano

Bidimensional H-Bond Network Promotes Structural Order and Electron Transport in BPyMPs Molecular Semiconductors: A Computational Study

Antonio De Nicola,[a] Andrea Correa,[b] Andrea Giunchi,[c] Luca Muccioli,[c] Gabriele D'Avino,[d] Junji Kido[a] and Giuseppe Milano[a,e]

[a] Department of Organic Device Engineering, Graduate School of Science and Engineering, Yamagata University 4-3-16 Johnan, Yonezawa, Yamagata 992–8510, Japan

[b] Dipartimento di Scienze Chimiche, Università di Napoli Federico II, Complesso Monte S. Angelo, I-80126 Napoli, Italy

[c] Dipartimento di Chimica Industriale "Toso Montanari", Università di Bologna, I-40136 Bologna, Italy

[d] Grenoble Alpes University, CNRS, Grenoble INP, Institut Néel, 25 rue des Martyrs, 38042 Grenoble, France

[e] Dipartimento di Chimica e Biologia "Adolfo Zambelli", Università degli Studi di Salerno, I-84084 Fisciano, Italy

ABSTRACT: The presence of a hydrogen bond (H-Bond) network has been proved to impact significantly the OLED devices efficiency by promoting molecular orientation and structural anisotropy in thin films. The design of specific compounds to control H-Bond network formation in an amorphous material, and hence to improve OLED performances, is needed. A successful example is given by the bi-pyridyl based family n-type of organic semiconductors named BPyMPM. The experimental evidences demonstrated a surprisingly higher electron mobility in thin film composed of B4PyMPM (B4), which is almost two order of magnitude higher than mobility measured for very similar member of the family, B2PyMPM (B2). We present a comprehensive computational study, where classical and ab-initio methods were combined, to investigate the 2D H-Bond network in B4 and B2 thin films. The results indicate that B4 forms a larger number of intermolecular C-H···N hydrogen bonds which promote a higher orientational and positional order in B4 films and superior electron transport properties.

1. INTRODUCTION

The Organic Light Emitting Diode research field has constantly grown in the last 35 years: Scopus web archive counts roughly 12000 publications from 1994 to 2020, while the number of publications per year is still increasing.[1]

Nowadays OLEDs dominate the display market and show promise for a similar success in lighting applications in the near future, owing to the high brightness and the low power consumption they can offer. New generation OLEDs are produced by vapor-deposition of organic materials which form layers, in which the molecular orientation is documented to be a key property capable to improve outcoupling and charge transport efficiency.[2–10]

The vapor deposition process allows to produce smooth films, with a control of film thickness on nanometer length scale, by condensing molecules from the gas phase onto a temperature-controlled substrate,[11] but offers much less control on molecular orientation and crystallinity, which are governed by a complex interplay between kinetic and thermodynamic effects, often substrate-dependent.[12,13] A viable strategy to maximize the thermodynamic thrust is to design molecules with specific shapes and functional groups that promote highly directional supramolecular interactions.

In this context, Prof. Yokoyama and co-workers demonstrated the general relationship between the structural anisotropy of a molecule and its orientational order and preferred alignment direction in a thin solid film.[14,15] In another series of studies, intermolecular C-H···N hydrogen bonds were exploited for driving the supramolecular assembling, by designing molecules containing multiple pyridine rings properly arranged in order to maximize intermolecular interactions that promote long-range structural order. References missing?

This strategy was showed to be successful and several molecules were demonstrated to form flat surfaces and regular stacking through self-assembly.[5–7,16] Moreover, the presence of a bidimensional H-bonds network promotes anisotropic optical properties, like the refractive index and extinction coefficient k, and a non-negligible electron mobility.[6] Remarkably, a difference of about two orders of magnitude in the electron mobility, from time-of-flight measurements, was found between vacuum deposited film composed of B4 ($\sim 10^{-4} cm^2 V^{-1} s^{-1}$) and B2 ($\sim 10^{-6} cm^2 V^{-1} s^{-1}$), respectively,[6] whose chemical structure is reported in Figure 1.

The understanding of the driving forces regulating molecular orientation is mandatory to optimize material properties, such as charge transport, and to design processes and/or compounds to improve device efficiency. In this matter, the molecular dynamics (MD) at atomic resolution is a powerful computational method able to rationalize the microscopic origin of the molecular preferred orientation.[17–26] Several studies have been reported to successfully study interfacial properties and molecular arrangement of numerous compounds used in OLED materials.[17,18,20,27] For a general description of the challenges and the strategies currently used in the computational modelling of

OLED materials, we refer the interested reader to a recent perspective [19] and the references therein.

In the present study, density functional theory (DFT) calculations and all-atom MD simulations are combined to investigate the molecular orientation of B4 and B2 in thin films as final aim. The role of the hydrogen bond network and its consequences on the molecular geometries and electrical properties are investigated. The paper is organized as follows: in the Methods and Models section the atomistic model description, force-field optimization, simulation protocol and computational details are reported. The structural and charge properties calculated from MD simulations are discussed and compared with experiments in the Results and Discussion section, while the main results are summarized in the Conclusion section.

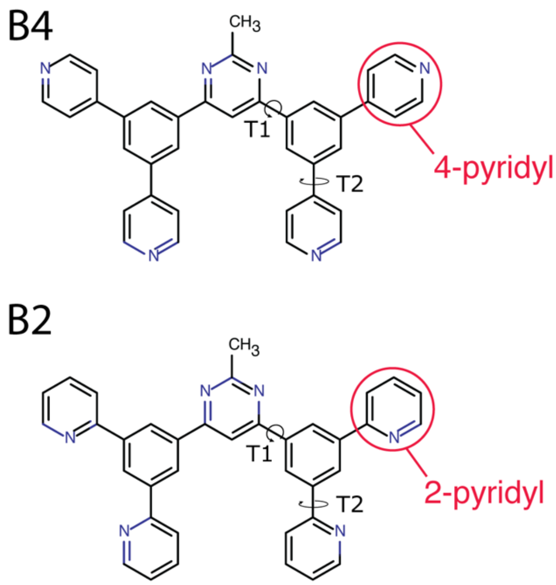

Figure 1. Chemical structure of B4 and B2 molecules. The different position of nitrogen atoms in the 4- and 2-pyridyl rings are indicated. In the following sections of the paper the dihedral angles φ_{T1} and φ_{T2} are also indicated.

2. METHODS AND MODELS

2.1 Molecular Dynamics Simulations. All the atomistic simulations reported in the paper were performed by using the GROMACS 5.0 simulation package.[28,29] A time step of 2 fs has been employed for all simulations. The temperature, in both NVT and NPT ensembles, has been held constant at 298 K by using a stochastic velocity rescaling algorithm[30] with a characteristic coupling time $\tau_T = 0.02$ ps; moreover, in the NPT ensemble the pressure has been kept constant at 1 atm by using the Berendsen barostat[31] (pressure coupling time $\tau_P = 0.2$ ps, compressibility of $1 \cdot 10^{-5}$ bar^{-1}, anisotropic scaling of box sides with the same τ_P value for x, y, z directions). All the bonds involving hydrogen atoms have been constrained using the LINCS algorithm.[32] Lennard-Jones interactions were calculated by using a cut-off distance of 1.4 nm, while electrostatic interactions have been treated with the Particle Mesh Ewald algorithm[33] with a grid spacing of 0.1 nm. System compositions and total simulation times are listed in Table 1.

Table 1. Characteristics of the simulated systems.

System	No. Molecules	Molecule Type	Ensemble	Average Box Length [x,y,z] (nm)	Time (ns)
Bulk	128	B4PyPTZ	NPT	5.382 ± 0.1, 3.514 ± 0.08, 5.443 ± 0.1	100
Bulk	128	B4	NPT	4.698 ± 0.1, 3.596 ± 0.1, 5.701 ± 0.12	100
Bulk	128	B2	NPT	5.102 ± 0.1, 3.587 ± 0.1, 5.567 ± 0.17	100
Film	128	B4	NVT	4.751, 3.627, 25.706	350
Film	128	B2	NVT	5.069, 3.561, 25.566	350

2.2 Atomistic Model. We adopted the atomistic OPLS force field (FF), developed by Jorgensen in 1996,[34] except for soft aryl-aryl torsions. These torsions and their energy barriers are fundamental in determining the molecular shape and must be described accurately for a correct modeling.[35] For instance, a recent extension of the OPLS-AA has been optimized to improve the description of inter-ring torsions[36] for molecules containing biaryl groups. Following these guidelines, we made a reparameterization of the Fourier coefficients used in the Fourier series sum describing the torsional energy profile (see eq. S4 of Supporting Information). The torsional energy profiles for φ_{T1} and φ_{T2} dihedrals were calculated (see Figure 1 for their definition). The geometries of B4 and B2 molecules have been optimized at different fixed aryl-aryl angles (with steps of 10º), at PBE0/6-311G** level,[37–39] using Gaussian09.[40] By fitting the torsional energy profile from DFT calculations of φ_{T1} and φ_{T2} dihedral angles, Fourier coefficients are obtained. The comparison between torsional energy profiles at DFT and FF level is reported in the Supporting Information together with the full list of FF parameters and the functional forms of bonded and non-bonded interactions.

2.3 Sample Preparation. The thin films of B4 or B2 compounds, prepared via vacuum deposition, possess to some extent an ordered structure, presumably due to a columnar arrangement favored by the presence of a bidimensional H-bond network.[6] Since the structural information in the solid state of B4 and B2 is not available, we built thin films initial configurations starting from the experimental crystal structure of a molecule, B4PyPTZ, having optical properties and chemical structure similar to B4 and B2. The crystallographic unit cell[5] of B4PyPTZ, containing 16 molecules, has been replicated

$2 \times 2 \times 1$ times along in *a, b, c* directions to build a supercell composed of 128 molecules.

The crystalline structure of B4PyPTZ is characterized by molecules stacked in columns. Each molecule belonging to a column is oriented in a way leaving the nitrogen atoms of terminal pyridine rings pointing toward the exterior of the column. The peculiar position of nitrogen atoms maximizes the probability to form of intermolecular H-bonds between adjacent columns, forming a bidimensional H-bond network.[5]

The stability of B4PyPTZ sample has been checked performing a MD simulation in the NPT ensemble employing the OPLS-AA force field with the tuned torsional potential for φ_{T1}, φ_{T2} angles. The equilibrium mass density obtained from the MD simulation (1278 kg/m$^3 \pm 5$ kg m^{-3}) slightly underestimates the experimental density[5] of about 3%. However, the deviation from the density experimental value is similar to those observed for the majority of organic molecules (2 - 4%) modelled by using OPLS force field.[36,41–44] Besides, the lattice constants (*a, b, c*) of crystalline structure are reproduced within an error of +1.9%. The time behavior of the mass density and the X-Ray pattern calculated on the equilibrium structure are reported in the Supporting Information.

The equilibrium structure of the B4PyPTZ supercell was used as initial coordinate set to build B4 and B2 systems. The description of the procedure employed to build systems and further details about it are reported in the Supporting Information.

NPT simulations revealed a difference in the equilibrium mass density between the two bulk systems, even if the only difference between the two molecules lies in the position of nitrogen atoms in the pyridine rings (Figure 1). Starting from initial configurations, at the same density for both molecules, the bulk of B4 reaches a slightly higher equilibrium density (1197 ± 5 kg m-3) than B2 (1176 ± 5 kg m-3) revealing a more efficient packing (time behavior of mass density is reported in Figure S8 of Supporting Information).

2.4 Electronic Structure Calculations. Most organic semiconductors with mobilities below ~1 cm^2/Vs are characterized by thermally activated hopping-like transport. The most popular, semiclassical rate equation for charge hopping is due to Marcus[45] (Eq. 1), stating a proportionality between the rate between two molecules i and j and the square of the intermolecular electronic coupling J_{ij}, and an Arrhenius-like exponential dependence with activation barrier of $\left(\Delta G_{ij} + \lambda\right)^2/(4\lambda)$:

$$k_{ij} = \frac{2\pi}{\hbar}\frac{J_{ij}^2}{\sqrt{4\pi\lambda k_B T}}\exp\left[-\frac{\left(\Delta G_{ij}+\lambda\right)^2}{4\lambda k_B T}\right] \qquad (1)$$

Where $\lambda = \lambda_i + \lambda_s$ is the total reorganization energy, quantifying the dynamic energetic fluctuations and including both the internal (λ_i) and environmental contribution (λ_S); ΔG_{ij} is the difference between the molecular site energies (averaged over dynamic fluctuations) and eventually including the effect of an applied electric field. For electron transport, the site energies correspond to the electron affinity with reversed sign, i.e.

$\Delta G_{ij} = -EA_j + EA_i$.

The site energy of a given molecule includes an intramolecular and an environmental component[46]:

$$EA = EA_{gas} - \Delta \qquad (2)$$

The term EA_{gas} corresponds to the electron affinity of the isolated molecule, and we approximate it with the LUMO energy, E_{LUMO}. The environmental component Δ is instead obtained with classical microelectrostatic (ME) calculations using MESCal code,[47] in which molecules interact through forces between atomic permanent charges and atomic induced dipoles, the latter requiring a self-consistent treatment of mutual interactions. The environmental contribution to site energies can be further partitioned into an electrostatic (Δ_E) and an introduction (Δ_I) term, $\Delta = \Delta_E + \Delta_I$. In particular, Δ_E corresponds to the energy to charge a molecule in the electrostatic potential of the permanent and induced multipoles of the surrounding molecules in the neutral sample, while Δ_I accounts for the dielectric screening of the added charge by the polarizable medium.[48] The induction term Δ_I affects the absolute values of the energy levels, typically increasing the EA by ~ 1 eV, but it is essentially isotropic and then contributes only marginally to the spread of the transport levels.[46] Then, this term is here disregarded, since our primary interest is the estimation of energetic disorder.

Our samples are characterized by the presence of structural disorder which may strongly affect the energetics of localized charge carriers (see e.g. ref. [49] for a discussion of different effects in play). In fact, each molecule experiences a different electrostatic environment, and this leads to a broad distribution of charge transport levels. These distributions often feature an approximately Gaussian shape, whose standard deviation σ is taken as a measure of the energetic disorder. The broadening of transport levels has been estimated upon sampling the EA over all the molecules, and for 11 thin film MD configurations. This allows us also to compute the static (or positional) and dynamic nature in of the energetic disorder. To such an aim, we define the average $\bar{x}_m$ and the variance σ_m^2 of the energy of molecule m over different configurations. Static and dynamic disorder are then computed as $\sigma_{static=}\sqrt{\langle(\bar{x}_m - \langle x\rangle)^2\rangle}$ and $\sigma_{dynamic=}\sqrt{\langle\sigma_m^2\rangle}$, respectively, where angle brackets denote the average over the molecules in the sample. It can be shown that $\sigma_{total}^2 = \sigma_{static}^2 + \sigma_{dynamic}^2$.

For the parameterization of the ME method, molecular polarizability and ESP charges for the neutral molecule and the anion have been obtained at the equilibrium geometry by PBE0/cc-pVTZ DFT calculations using Gaussian16.[50] The simulated samples were treated as thin films, applying periodic boundary conditions in two dimensions (x, y) and constructing supercells of the original samples. We have verified that a cutoff of 44 nm (about 8 times the average thickness of the samples) ensures a proper convergence of electrostatic interactions, i.e. within 50 meV for absolute energies and 5 meV for energy differences between sites. Electronic couplings were calculated for every pair of molecules ("dimers", having at least two atoms at distance lower than 7 Å) in a single configuration of the B2 and B4 samples. Calculations were carried out at DFT level B3LYP/6-31G(d), ORCA code[51] with the dimer projection method.[52] The intermolecular reorganization energies λ_i for B2 and B4 were calculated using the four-point method[53] via PBE0/cc-pVTZ calculations , and amount to 0.3 eV for B2 and 0.32 for B4, respectively. These values are considerably larger than the one of the prototypical n-type organic semiconductor C60 fullerene.[54,55]

3. RESULTS

3.1 B4 and B2 Films. Since the experimental fabrication of B4 and B2 films is made by vacuum deposition, to mimic as much as possible experimental conditions MD simulations of the bulk/vacuum interface have been performed. The intent is to include the effect of the vacuum/film interface affecting molecular geometries and structural properties. To this aim, four independent configurations of B2 and B4 have been extracted from MD trajectories of bulk phase (a .configuration every 20 ns of the last 80 ns of each trajectory) and used as a starting coordinate set to simulate vacuum/bulk interface systems. The vacuum interface has been built by increasing the box side (z) by 20 nm. Then, MD simulations in NVT ensemble have been performed for each independent configuration. Representative snapshots of equilibrium configurations of B2 and B4 systems are reported in Figure 2.

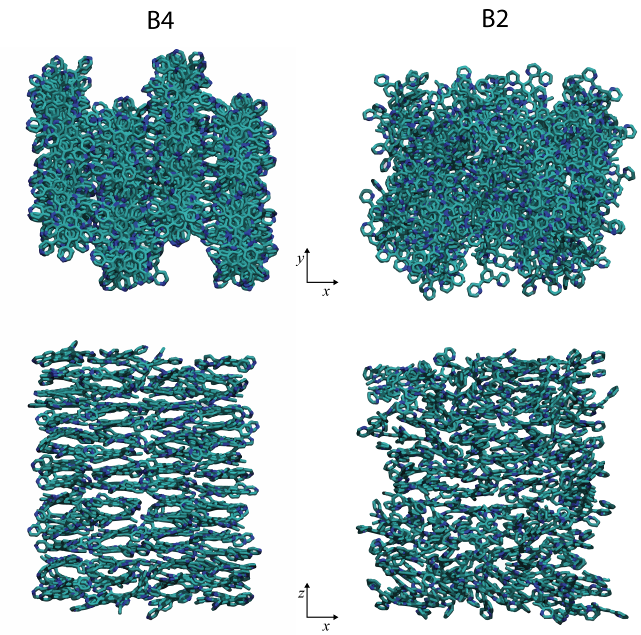

Figure 2. Snapshots representative of the equilibrium configuration of B4 and B2 systems. Nitrogen atoms are represented in blue, carbons in cyan and hydrogens in white. The vacuum/bulk interface is perpendicular to z direction.

The visual inspection of equilibrium configurations reveals a well-defined columnar structure for the B4 system (left side of Figure 2). Instead, B2 molecules (right side of Figure 2) are much more disorderly stacked on each other, and, many of them appear tilted with the respect to the normal direction (z) of the bulk/vacuum interface. A more quantitative indication is gained by computing the X-Ray powder pattern and the radial distribution function (g(r)). As can be seen from panel A in Figure 3, both X-Ray traces show a peak at q~ 1.53 Å^{-1}, corresponding to molecular π-stacking distance. The B4 profile shows a sharp peak at this position, which is comparable with the experimental spacing of ~ 4 Å measured on a thin film of B4 material.[6] The comparison with the broader peak found for B2 indicates a decrease of positional order along the stacking direction for the latter system. The difference in the positional order between B2 and B4 systems is confirmed by the g(r) displayed in Figure 3B.

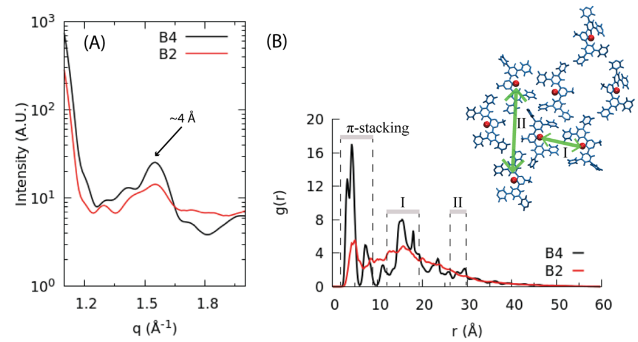

Figure 3. (A) X-Ray powder pattern is calculated using CuK_{α} radiation (λ = 1.5418 Å) as in the experiments.[6] Using the last 80 ns of trajectories, structure factor patterns for B4 (black) and B2 (red) were calculated by using the ISAACS package.[56] (B) Radial distribution functions g(r) calculated for the core hydrogens. Explicit assignment of the main peaks is reported in the plot. A snapshot of B4 system, counting eight molecules belonging to adjacent columns is reported to outline the hexagonal packing.

These functions have has been computed by considering only the hydrogen atom belonging to the central pyrimidine ring; those atoms are shown as red spheres in the snapshot of Figure 3B. Due to its peculiar position, the pyrimidine hydrogen is a convenient choice to characterize structural properties at molecular (π-stacking) and bulk scales (hexagonal packing in case of B4). As can be seen from the comparison between B2 and B4 curves, it is clear that B4 has much higher positional order, in particular in the region of π-stacking (~ 3-5 Å) which is fundamental for promoting electron transport, with peaks about three times more intense than for B2. At larger distances, the B4 g(r) shows two main peaks, region I at ~ 1.5 nm and region II at ~ 2.8 nm, which represent the characteristic interplanar distances of the nearly hexagonal packing. Instead, B2 shows a featureless broad halo in the same region, which indicates lower structuration. Additional snapshots highlighting the hexagonal packing are reported in Figure S10 of Supporting Information. Since structural order and molecular orientation are correlated, a high positional order of B4 structure should correspond to a high orientational order, too. The regularity in molecular orientation can be computed using the orientational order parameter (P_2), which is defined as:

$$\langle P_2 \rangle = \frac{3\langle cos^2\theta \rangle - 1}{2} \qquad (4)$$

where θ is the angle between an arbitrary molecular axis $\boldsymbol{m}$ (see definition in Figure 4A) and a reference direction $\boldsymbol{z}$. The angle bracket indicates the ensemble average. If we choose the molecular axis in the pyrimidine plane as in reference [6], when every molecular axis is oriented parallel to the $\boldsymbol{z}$ vector (the normal to the surface), and hence in a perfect edge-on configuration, P_2 is equal to 1, for an isotropic distribution of orientations P_2 equals to 0 and for a perfect face-on distribution, P_2 is equal to -0.5.

In Figure 4B, computed and experimental P_2 are compared: while for B2 the orientational order is slightly overestimated with respect to the measured value, the calculated values show the same trend of the experimental data, with B4 being more ordered that B2. More in detail, we observe that B4 molecules have a more pronounced "face-on" orientation than B2. The tendency to form well-ordered columnar stacks is beneficial for key properties such as charge transport and efficiency in OLEDs devices, as reported by Kido and co-workers.[4–7,57]

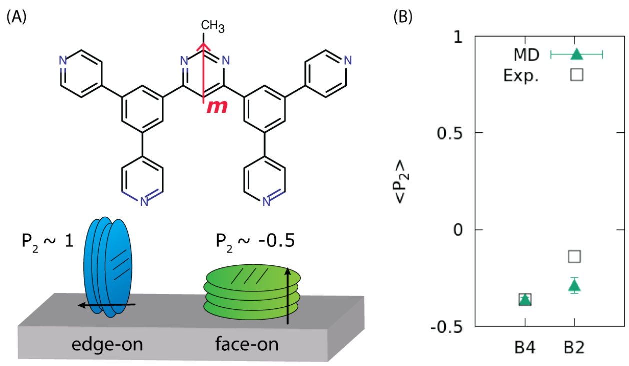

Figure 4. (A) scheme showing the definition of molecular axis ***m*** (red arrow) and face-on, edge-on orientation on a substrate. (B) P_2 calculated from MD simulations (solid triangles) and from experiments [6] (open squares).

3.2 Hydrogen Bonds. The higher solubility of B4 in chloroform with a small amount of methanol is an evident experimental proof of the strongest H-bond network formed by B4 with respect B2.[6] In addition, the presence of a strong bidimensional H-Bond network was also demonstrated by scanning tunneling microscopy (STM) experiments carried out at the interface between a solution of B4 and a graphite surface.[58–62]

To detect H-bonds features, simulation trajectories have been analyzed in detail. In particular, B2 and B4 molecular structures display several possible (weak) H-bond acceptor (A) and donor (D) sites (definitions in Figure 5A). During the simulation, a hydrogen bond is counted when two geometrical conditions are simultaneously satisfied:[63] First, the distance between A and D must be shorter or equal to r_C cut-off distance of 0.3 nm; second, the angle $\theta_{(A-H-D)}$ must be larger than $\theta_{cut-off} = 120º$. We have tested different cut-off distances and cut-off angles in the H-Bond counting to verify the correct applicability of the used values proposed in reference [63]. Additional analyses are reported in the Supporting Information.

In agreement with the experimental evidences,[6,58–62] we have found a higher average number of H-bonds/molecule (~ 2.5) for B4 with respect to B2 (1.5), as shown in the histogram in Figure 5B. According to a geometrical criterion based on the π-stacking distance (~ 4 Å), hydrogen bonds were also labelled as in-plane or out-of-plane. If the D-A distance along the normal direction of bulk/vacuum interface z) between D and A is longer than 4 Å, the H-Bond is counted as out-of-plane; for longer distances the H-Bond is counted as out-plane, or in other words the bond is roughly coplanar with the molecular planes. The fraction of in-plane bonds is reported in Figure 5, panel C, alongside the intra molecular H-bond fraction in panel D. In case of B4, the majority of H-bonds is formed between molecules laying a same plane (~ 0.87), instead, a lower fraction (~ 0.58) is found for B2. Furthermore, B4 molecules do not form, in practice, intramolecular H-bonds, while B2 has a noticeable amount of them (nearly 0.12, Figure 5D). These results, in addition to previous structural results (including order parameter, X-Ray pattern, g(r) and mass density) confirm the interpretation of the assembly given by Kido and co-workers[6] and also discussed in the interpretation of B4 two dimensional structures. [58–62] In particular, B4 pyridine nitrogen atoms are positioned at the very edge of the molecule, and then favoring in-plane connections between pairs of coplanar molecules via intermolecular H-bonds, and to form a bidimensional network. The ortho position of nitrogen atoms in pyridine rings in B2 instead implies a rotation of those rings to maximize the number of intermolecular H-Bonds. However, even if a 2D H-bond is formed, such a rotation of reduces the planarity and, as a consequence, the packing ability of B2. This is clearly reflected by the lower mass density reached by B2 bulk, reduced structural order and lower number of H-Bonds per molecule with respect to B4. In addition to those evidences, the distributions of φ_{T1} and φ_{T2} dihedral angles suggest a slightly higher planarity for B4 (Figure S11 of Supporting Information).

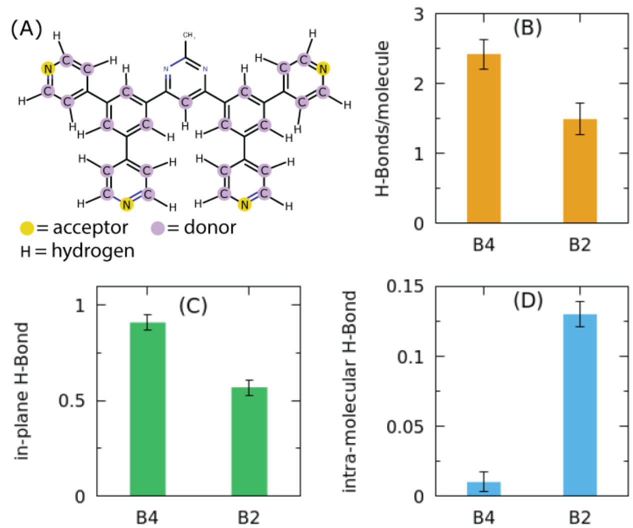

Figure 5. (A) definition of hydrogen bond acceptor and donor sites for B4. (B) average number of H-bonds/molecule. (C) In-plane H-Bond fraction, and (D) intra molecular H-bonds fraction. Data has been computed on the last 35 ns of MD trajectories.

3.3 Electron Transfer Parameters. As already mentioned, Kido and coauthors[6] measured the electron mobility of B2 and B4 with the time of flight technique, obtaining at room temperature values of the order of 10^{-6} and 10^{-4} $cm^2V^{-1}s^{-1}$, respectively. In this section, exploiting the atomic resolution of the system morphologies provided by MD simulations, we aim at establishing a link between structural and electronic properties, and analyze the factors that contribute to the large offset between B2 and B4 mobility.

We begin the comparison of the charge transport properties of the two systems by inspecting the distributions of electron affinities, i.e. the density of states available to charge carriers. The histograms in Figure 6 clearly show two main differences: first, B4 has an electron affinity larger than B2, which is a positive characteristics because it improves the air stability of the semiconductor[64] and facilitates a possible doping by electron donating impurities. Moreover, the distribution of electron affinity for B4 is narrower than the one for B2. Again, this goes in favor of superior electron transport in the B4 system, since its standard deviation σ is usually taken as a measure of the energetic disorder, which in turn is one of the main limiting factors for charge mobility.[49]

For a quantitative analysis of the energetic disorder and its nature, we then analyzed the standard deviations of EA, E_{LUMO}, and Δ_E, reported in Table 2. It is also useful to partition the disorder in a static (or positional) term, that does not change in time and affects the ΔG_{ij} values in eq. 1, and a dynamic one which instead has to be included in the reorganization energy.[54] Both static and dynamic terms negatively impact charge transfer rates, ultimately reducing the mobility, although each with a distinct physical mechanism.

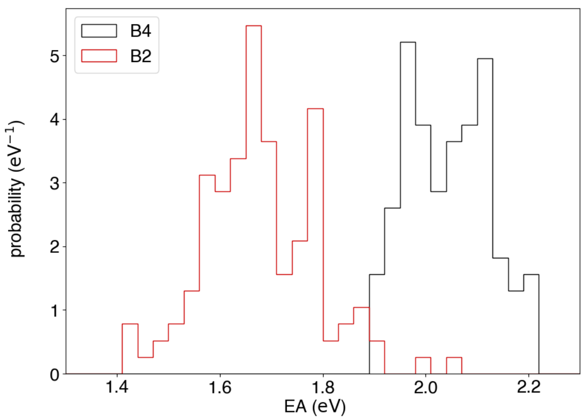

Figure 6. Distribution of electron affinities for B4 and B2, averaged on eleven MD configurations. Individual values were obtained as $EA = -(E_{LUMO}+\Delta_E)$ by DFT and microelectrostatic calculations.

We note that the calculated static disorder of EA is larger for B2, and qualitatively in line with the experimental values, which were obtained by fitting mobility dependence on electric field and temperature with an empirical but well established equation for amorphous semiconductors[65] (0.091 and 0.076 eV for B2 and B4, respectively[6]). This observation is in line with the higher structural order present in B4 samples. The amount of dynamic disorder is instead rather similar for the two systems, yet again slightly larger for B2. These room-temperature energetic fluctuations correspond to a reorganization energy $\lambda = \frac{\sigma^2_{dynamic}}{k_B T}$ about 0.12 eV higher for B2. From Table 2 it can be further seen that the difference in energetic disorder between the two systems, both for the static and dynamic component, is sourced from the environmental electrostatic contribution Δ_E, while the fluctuations of the LUMO energies are quite similar, albeit again a bit larger for B2.

To explain the higher disorder of the energy levels in B2 and its chiefly dynamic nature, let us consider the four terminal pyridine units: any thermally activated rotation about the pyridine-phenyl bond marginally affects the electrostatic layout of B4, where the local dipole associated with the pyridine nitrogen is coaxial with the bond. On the other hand, pyridine rotations can produce a rather large variation of charge distribution for B2, where the dipole is off-axis. This makes that, for B2, a given amount of dynamic conformational disorder translates in more important variations of the electrostatic landscape felt by the charge carriers. The argument is strengthened by the DFT calculation of the gas phase molecular dipoles along the trajectories, that yields larger values and fluctuations for B2: 2.9 ± 1.3 D versus 0.8 ± 0.3 D for B4.

Table 2: Averages of intramolecular ($\boldsymbol{E_{\mathrm{LUMO}}}$), intermolecular ($\Delta_{\boldsymbol{E}}$), and total electron affinities ($\boldsymbol{EA = -E_{\mathrm{LUMO}} - \Delta_E}$), and corresponding standard deviations separated in static and dynamic contributions $\boldsymbol{\sigma_{static}}$ and $\boldsymbol{\sigma_{dynamic}}$. Average energies are in eV, standard deviations in meV.

B2	average	σ_{total}	σ_{static}	$\sigma_{dynamic}$
E_{LUMO}	-1.681	97	50	83
Δ_E	0.000	181	124	132
EA	1.681	183	111	145
B4	average	σ_{total}	σ_{static}	$\sigma_{dynamic}$
E_{LUMO}	-2.201	81	30	75
Δ_E	0.156	129	67	110
EA	2.046	156	81	134

We now focus our attention on the magnitude and fluctuations of intermolecular electron-transfer couplings J, representing the pre-exponential factor in equation 1, and on their relationship with the structural organization in the simulated samples. Figure 7A, compares the magnitude and directionality of intermolecular couplings between the two materials, reporting the absolute value of J, computed for molecular pairs in our MD samples, against r_z/r (gray dots), being r the module of the intermolecular distance and r_z its z-axis component. Charge transfer couplings are highly anisotropic in both systems (see also Figure S16), attaining appreciable values only when the intermolecular vector is parallel to the stacking direction ($r_z/r > 0.6$). As better appreciated by the average values of $|J|$ over r_z/r intervals (red squares), the magnitude of the couplings is significantly larger in B4 than in B2, and this difference determines a superior electronic connectivity with respect to B2. This quantity, shown in Figure 7B, corresponds to number of neighbors that, on average, is connected to each molecule by a coupling exceeding a given value of $|J|$. The two systems approach in a very different way the connectivity of 2 characteristic of an ideal 1D semiconductor, with e.g. B4 attaining the value of 1.5 with couplings of 41 meV, and B2 only for $|J|$=12 meV.

The superior charge transfer properties of B4 as compared to B2 are completely unexpected at the molecular level, given the similar structure and the nearly identical LUMO orbitals (see inset Figure 7A) of the two molecules.[6] We expect that the difference between the two materials may be due to the better supramolecular packing of B4 discussed above. To prove this hypothesis with an "alchemical" experiment, impossible to perform with real systems, we have computed the intermolecular couplings for a fictitious B4 phase, obtained from the atomic coordinates of the B2 sample by switching the positions of the N atom and one CH group in the peripheral pyridine rings. Figure 7C, compares the couplings of this hypothetical sample, labelled "B4 < B2", with the original B2 ones. This plot reveals a nearly perfect correlation between the two data sets (Pearson coefficient R=0.994), demonstrating that the differences between the charge transport properties of the two materials does not arise from the chemical structure. It has instead to be ascribed to the better molecular organization in B4, in turn resulting from the presence of a two-dimensional H-bond network.

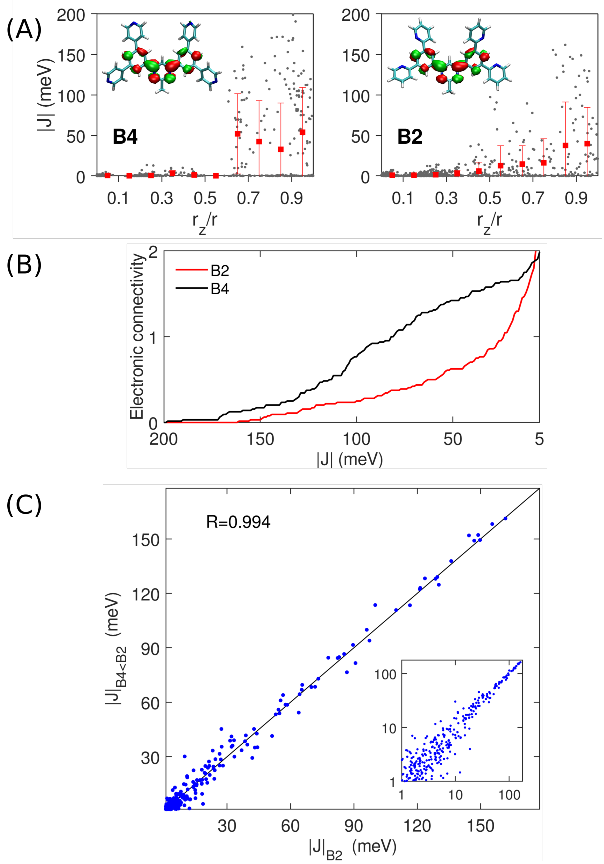

Figure 7. (A) Electron-transfer couplings as a function of the normalized projection of the intermolecular vector distance $\boldsymbol{r}$ along the stacking axis z. Gray dots show the couplings computed for molecular pairs extracted from the MD sample, red squared (error bars) show the mean value (standard deviation) over intervals of r_z/r. LUMO orbitals of B4 and B2 are shown as insets. (B) Electronic connectivity, i.e. average number of neighbors per molecule having an electronic coupling larger than the abscissa value. (C) Correlation between the couplings of B2 and those of a fictitious B4 sample obtained modifying the atomistic morphologies of B2 (see text). The quadrant bisector (black line) is shown as a guide for the eye. The same plot in a log-log scale in shown as an inset.

4. CONCLUSIONS

Combining DFT calculations and MD all-atom simulations we investigated the role of intermolecular hydrogen bonds in the molecular orientation, stacking and electron carrier mobility of thin films composed of pyridine-based molecules B2 and B4.

The only difference between the B4 and B2 chemical structure lies in the position of nitrogen atoms in the four outer pyridine rings, which is surprisingly sufficient for causing a huge difference in the optical and electron transport properties, as experimentally proved. We found that B4 has a higher capability to connect with adjacent molecules, by intermolecular hydrogen bonds, compared with B2 (2.5 vs 1.5 bonds per molecule). The stronger 2D H-bond network formed for B4 is sufficient to stabilize a supramolecular organization in which molecules form ordered layers and columns.

The calculation of essential electron transport parameters, such as reorganization energies, site energies, and electronic couplings revealed that the microscopic origin of the higher electron mobility of B4 with respect to B2 has its roots in lower reorganization energy and electrostatic disorder and, more importantly, in the superior morphology promoted by the hydrogen bond network.

On a general vein, our findings disclose how intermolecular hydrogen bond interactions promote structural order in molecular thin films, ultimately improving their electron transport properties. The engineering of these weak interactions offers viable opportunities for the rational design of new materials with improved performances in OLED applications.

These findings provide a detailed molecular view of the H-bond interactions governing spatial organization and charge transport in thin films. The knowledge gained from the study is of primary importance in developing new materials and/or to improve performances of OLED devices.

ASSOCIATED CONTENT

Supporting Information

Model description, Force-Field parameter tables, parameterization procedure for soft aryl-aryl torsions. Additional analysis of crystalline system of B4PyPTZ, procedure description for the thin film preparation of B4 and B2. Additional figures and analysis for H-bond and charge transport. The Supporting Information is available free of charge on the ACS Publications website.

ABBREVIATIONS

B4 = (4,6-bis(3,5-di(pyridine-4-yl)phenyl)-2-methylpyrimidine
B2 = (4,6-bis(3,5-di(pyridine-2-yl)phenyl)-2-methylpyrimidine

AUTHOR INFORMATION

Author Contributions

The manuscript was written through contributions of all authors. All authors have given approval to the final version of the manuscript.

Funding Sources

Any funds used to support the research of the manuscript should be placed here (per journal style).

Notes

Any additional relevant notes should be placed here.

ACKNOWLEDGMENT

GM and ADN acknowledge the computing resources and the related technical support used for this work have been provided by CRESCO/ ENEAGRID High Performance Computing infrastructure and its staff. CRESCO/ENEAGRID High Performance Computing infrastructure is funded by ENEA, the Italian National Agency for New Technologies, Energy and Sustainable Economic Development and by Italian and European research programs, see ww.cresco.enea.it/English/ for information.
LM acknowledges funding through PRIN project "From natural to artificial light-harvesting systems: unveiling fundamental processes towards a bio-inspired materials design" (HARVEST) protocol 201795SBA3.

REFERENCES

(1) scopus.com https://www.scopus.com/ (accessed May 19, 2020).
(2) Marcato, T.; Shih, C. J. Molecular Orientation Effects in Organic Light-Emitting Diodes. *Helv. Chim. Acta* **2019**, *102* (5).
(3) Boehm, B. J.; Nguyen, H. T. L.; Huang, D. M. The Interplay of

Interfaces, Supramolecular Assembly, and Electronics in Organic Semiconductors. *J. Phys. Condens. Matter* **2019**, *31* (42).
(4) Ohisa, S.; Pu, Y.-J.; Yamada, N. L.; Matsuba, G.; Kido, J. Molecular Interdiffusion between Stacked Layers by Solution and Thermal Annealing Processes in Organic Light Emitting Devices. *ACS Appl. Mater. Interfaces* **2015**, *7* (37), 20779–20785.
(5) Watanabe, Y.; Sasabe, H.; Yokoyama, D.; Beppu, T.; Katagiri, H.; Pu, Y. J.; Kido, J. Simultaneous Manipulation of Intramolecular and Intermolecular Hydrogen Bonds in N-Type Organic Semiconductor Layers: Realization of Horizontal Orientation in OLEDs. *Adv. Opt. Mater.* **2015**, *3* (6), 769–773.
(6) Yokoyama, D.; Sasabe, H.; Furukawa, Y.; Adachi, C.; Kido, J. Molecular Stacking Induced by Intermolecular C-H···N Hydrogen Bonds Leading to High Carrier Mobility in Vacuum-Deposited Organic Films. *Adv. Funct. Mater.* **2011**, *21* (8), 1375–1382.
(7) Watanabe, Y.; Yokoyama, D.; Koganezawa, T.; Katagiri, H.; Ito, T.; Ohisa, S.; Chiba, T.; Sasabe, H.; Kido, J. Control of Molecular Orientation in Organic Semiconductor Films Using Weak Hydrogen Bonds. *Adv. Mater.* **2019**, *31* (18), 1–8.
(8) Duhm, S.; Heimel, G.; Salzmann, I.; Glowatzki, H.; Johnson, R. L.; Vollmer, A.; Rabe, J. P.; Koch, N. Orientation-Dependent Ionization Energies and Interface Dipoles in Ordered Molecular Assemblies. *Nat. Mater.* **2008**, *7* (4), 326–332.
(9) Frischeisen, J.; Yokoyama, D.; Endo, A.; Adachi, C.; Brütting, W. Increased Light Outcoupling Efficiency in Dye-Doped Small Molecule Organic Light-Emitting Diodes with Horizontally Oriented Emitters. *Org. Electron.* **2011**, *12* (5), 809–817.
(10) Liehm, P.; Murawski, C.; Furno, M.; Lüssem, B.; Leo, K.; Gather, M. C. Comparing the Emissive Dipole Orientation of Two Similar Phosphorescent Green Emitter Molecules in Highly Efficient Organic Light-Emitting Diodes. *Appl. Phys. Lett.* **2012**, *101* (25), 253304.
(11) Ediger, M. D.; de Pablo, J.; Yu, L. Anisotropic Vapor-Deposited Glasses: Hybrid Organic Solids. *Acc. Chem. Res.* **2019**, *52* (2), 407–414.
(12) Ediger, M. D. Perspective: Highly Stable Vapor-Deposited Glasses. *J. Chem. Phys.* **2017**, *147* (21), 210901.
(13) Roscioni, O. M.; D'avino, G.; Muccioli, L.; Zannoni, C. Pentacene Crystal Growth on Silica and Layer-Dependent Step-Edge Barrier from Atomistic Simulations. *J. Phys. Chem. Lett.* **2018**, *9* (23), 6900–6906.
(14) Yokoyama, D.; Sakaguchi, A.; Suzuki, M.; Adachi, C. Horizontal Molecular Orientation in Vacuum-Deposited Organic Amorphous Films of Hole and Electron Transport Materials. *Appl. Phys. Lett.* **2008**, *93* (17).
(15) Yokoyama, D.; Sakaguchi, A.; Suzuki, M.; Adachi, C. Horizontal Orientation of Linear-Shaped Organic Molecules Having Bulky Substituents in Neat and Doped Vacuum-Deposited Amorphous Films. *Org. Electron.* **2009**, *10* (1), 127–137.
(16) Sasabe, H.; Tanaka, D.; Yokoyama, D.; Chiba, T.; Pu, Y.-J.; Nakayama, K.; Yokoyama, M.; Kido, J. Influence of Substituted Pyridine Rings on Physical Properties and Electron Mobilities of 2-Methylpyrimidine Skeleton-Based Electron Transporters. *Adv. Funct. Mater.* **2011**, *21* (2), 336–342.
(17) Yoo, D.; Song, H.; Youn, Y.; Jeon, S. H.; Cho, Y.; Han, S. A Molecular Dynamics Study on the Interface Morphology of Vapor-Deposited Amorphous Organic Thin Films. *Phys. Chem. Chem. Phys.* **2019**, *21* (3), 1484–1490.
(18) Youn, Y.; Yoo, D.; Song, H.; Kang, Y.; Kim, K. Y.; Jeon, S. H.; Cho, Y.; Chae, K.; Han, S. All-Atom Simulation of Molecular Orientation in Vapor-Deposited Organic Light-Emitting Diodes. *J. Mater. Chem. C* **2018**, *6* (5), 1015–1022.
(19) Olivier, Y.; Sancho-Garcia, J. C.; Muccioli, L.; D'Avino, G.; Beljonne, D. Computational Design of Thermally Activated Delayed Fluorescence Materials: The Challenges Ahead. *J. Phys. Chem. Lett.* **2018**, *9* (20), 6149–6163.
(20) Hu, T.; Han, G.; Tu, Z.; Duan, R.; Yi, Y. Origin of High Efficiencies for Thermally Activated Delayed Fluorescence Organic Light-Emitting Diodes: Atomistic Insight into Molecular Orientation and Torsional Disorder. *J. Phys. Chem. C* **2018**, *122* (48), 27191–27197.
(21) Muccioli, L.; D'Avino, G.; Zannoni, C. Simulation of Vapor-Phase Deposition and Growth of a Pentacene Thin Film on C60(001). *Adv. Mater.* **2011**, *23* (39), 4532–4536.
(22) Walters, D. M.; Antony, L.; De Pablo, J. J.; Ediger, M. D. Influence of Molecular Shape on the Thermal Stability and Molecular Orientation of Vapor-Deposited Organic Semiconductors. *J. Phys. Chem. Lett.* **2017**, *8* (14), 3380–3386.
(23) Antony, L. W.; Jackson, N. E.; Lyubimov, I.; Vishwanath, V.; Ediger, M. D.; De Pablo, J. J. Influence of Vapor Deposition on Structural and Charge Transport Properties of Ethylbenzene Films. *ACS Cent. Sci.* **2017**, *3* (5), 415–424.
(24) Lee, T.; Caron, B.; Stroet, M.; M. Huang, D.; L. Burn, P.; E. Mark, A. The Molecular Origin of Anisotropic Emission in an Organic Light-Emitting Diode. *Nano Lett.* **2017**, *17* (10), 6464–6468.
(25) Tonnelé, C.; Stroet, M.; Caron, B.; Clulow, A. J.; Nagiri, R. C. R.; Malde, A. K.; Burn, P. L.; Gentle, I. R.; Mark, A. E.; Powell, B. J. Elucidating the Spatial Arrangement of Emitter Molecules in Organic Light-Emitting Diode Films. *Angew. Chemie - Int. Ed.* **2017**, *56* (29), 8402–8406.
(26) Han, G.; Shen, X.; Yi, Y. Deposition Growth and Morphologies of C60 on DTDCTB Surfaces: An Atomistic Insight into the Integrated Impact of Surface Stability, Landscape, and Molecular Orientation. *Adv. Mater. Interfaces* **2015**, *2* (17), 1500329.
(27) Yoneya, M.; Matsuoka, S.; Tsutsumi, J.; Hasegawa, T. Self-Assembly of Donor–Acceptor Semiconducting Polymers in Solution Thin Films: A Molecular Dynamics Simulation Study. *J. Mater. Chem. C* **2017**, *5* (37), 9602–9610.
(28) Berendsen, H. J. C.; Van Der Spoel, D.; Van Drunen, R. GROMACS: A Message-Passing Parallel Molecular Dynamics Implementation PROGRAM SUMMARY Title of Program: GROMACS Version 1.0. *Comput. Phys. Commun.* **1995**, *91*, 43–56.
(29) Hess, B.; Kutzner, C.; van der Spoel, D.; Lindahl, E. GROMACS 4: Algorithms for Highly Efficient, Load-Balanced, and Scalable Molecular Simulation. *J. Chem. Theory Comput.* **2008**, *4* (3), 435–447.
(30) Bussi, G.; Donadio, D.; Parrinello, M. Canonical Sampling Throught Velocity Rescaling. *J. Chem. Phys.* **2007**, *126*, 14101.
(31) Berendsen, H. J. C.; Postma, J. P. M.; van Gunsteren, W. F.; DiNola, A.; Haak, J. R. Molecular Dynamics with Coupling to an External Bath. *J. Chem. Phys.* **1984**, *81* (8), 3684–3690.
(32) Hess, B.; Bekker, H.; Berendsen, H. J. C.; Fraaije, J. G. E. M. LINCS: A Linear Constraint Solver for Molecular Simulations. *J. Comput. Chem.* **1997**, *18* (12), 1463–1472.
(33) Darden, T.; York, D.; Pedersen, L. Particle Mesh Ewald: An Nlog(N) Method for Ewald Sums in Large Systems. *J. Chem. Phys.* **1993**, *98* (12), 10089–10092.
(34) Jorgensen, W. L.; Maxwell, D. S.; Tirado-Rives, J. Development and Testing of the OPLS All-Atom Force Field on Conformational Energetics and Properties of Organic Liquids. *J. Am. Chem. Soc.* **1996**, *118* (45), 11225–11236.
(35) Muccioli, L.; D'Avino, G.; Berardi, R.; Orlandi, S.; Pizzirusso, A.; Ricci, M.; Roscioni, O. M.; Zannoni, C. Supramolecular Organization of Functional Organic Materials in the Bulk and at Organic/Organic Interfaces: A Modeling and Computer Simulation Approach BT - Multiscale Modelling of Organic and Hybrid Photovoltaics; Beljonne, D., Cornil, J., Eds.; Springer Berlin Heidelberg: Berlin, Heidelberg, 2014; pp 39–101.
(36) Dahlgren, M. K.; Schyman, P.; Tirado-Rives, J.; Jorgensen, W. L. Characterization of Biaryl Torsional Energetics and Its Treatment In. *J. Chem. Inf. Model.* **2013**, *53*, 1191−1199.
(37) Petersson, G. A.; Bennett, A.; Tensfeldt, T. G.; Al-Laham, M. A.; Shirley, W. A.; Mantzaris, J. A Complete Basis Set Model Chemistry. I. The Total Energies of Closed-shell Atoms and Hydrides of the First-row Elements. *J. Chem. Phys.* **1988**, *89* (4), 2193–2218.
(38) Ernzerhof, M.; Perdew, J. P. Generalized Gradient Approximation to the Angle- and System-Averaged Exchange Hole. *J. Chem. Phys.* **1998**, *109* (9), 3313–3320.
(39) Petersson, G. A.; Al-Laham, M. A. A Complete Basis Set Model Chemistry. II. Open-shell Systems and the Total Energies of the First-row Atoms. *J. Chem. Phys.* **1991**, *94* (9), 6081–6090.
(40) Frisch, M.; Trucks, G. W.; Schlegel, H. B.; Scuseria, G. E.; Robb, M. A.; Cheeseman, J. R.; Scalmani, G.; Barone, V.; Mennucci, B.; Petersson, G. A. ea. Gaussian09 Revision D. 01. 2014.
(41) Chen, B.; Martin, M. G.; Siepmann, J. I. Thermodynamic

Properties of the Williams, OPLS-AA, and MMFF94 All-Atom Force Fields for Normal Alkanes. *J. Phys. Chem. B* **1998**, *102* (14), 2578–2586.
(42) Jorgensen, W. L.; Mcdonald, N. A. *Development of an All-Atom Force Field for Heterocycles. Properties of Liquid Pyridine and Diazenes'*; 1998; Vol. 424.
(43) Bernardes, C. E. S.; Joseph, A. Evaluation of the OPLS-AA Force Field for the Study of Structural and Energetic Aspects of Molecular Organic Crystals. *J. Phys. Chem. A* **2015**, *119* (12), 3023–3034.
(44) Moral, M.; Son, W.-J.; Sancho-García, J. C.; Olivier, Y.; Muccioli, L. Cost-Effective Force Field Tailored for Solid-Phase Simulations of OLED Materials. *J. Chem. Theory Comput.* **2015**, *11* (7), 3383–3392.
(45) Marcus, R. A. Electron Transfer Past and Future. *Advances in Chemical Physics*. January 1, 1999, pp 1–6.
(46) D'Avino, G.; Muccioli, L.; Castet, F.; Poelking, C.; Andrienko, D.; Soos, Z. G.; Cornil, J.; Beljonne, D. Electrostatic Phenomena in Organic Semiconductors: Fundamentals and Implications for Photovoltaics. *J. Phys. Condens. Matter* **2016**, *28* (43).
(47) D'Avino, G.; Muccioli, L.; Zannoni, C.; Beljonne, D.; Soos, Z. G. Electronic Polarization in Organic Crystals: A Comparative Study of Induced Dipoles and Intramolecular Charge Redistribution Schemes. *J. Chem. Theory Comput.* **2014**, *10* (11), 4959–4971.
(48) D'Avino, G.; Duhm, S.; Della Valle, R. G.; Heimel, G.; Oehzelt, M.; Kera, S.; Ueno, N.; Beljonne, D.; Salzmann, I. Electrostatic Interactions Shape Molecular Organization and Electronic Structure of Organic Semiconductor Blends. *Chem. Mater.* **2020**, *32* (3), 1261–1271.
(49) Gali, S. M.; D'Avino, G.; Aurel, P.; Han, G.; Yi, Y.; Papadopoulos, T. A.; Coropceanu, V.; Brédas, J.-L.; Hadziioannou, G.; Zannoni, C.; et al. Energetic Fluctuations in Amorphous Semiconducting Polymers: Impact on Charge-Carrier Mobility. *J. Chem. Phys.* **2017**, *147* (13), 134904.
(50) Frisch, M. J.; Trucks, G. W.; Schlegel, H. B.; Scuseria, G. E.; Robb, M. a.; Cheeseman, J. R.; Scalmani, G.; Barone, V.; Petersson, G. a.; Nakatsuji, H.; et al. Gaussian 16, Revision C.01. 2016.
(51) Neese, F. The ORCA Program System. *WIREs Comput. Mol. Sci.* **2012**, *2* (1), 73–78.
(52) Senthilkumar, K.; Grozema, F. C.; Bickelhaupt, F. M.; Siebbeles, L. D. A. Charge Transport in Columnar Stacked Triphenylenes: Effects of Conformational Fluctuations on Charge Transfer Integrals and Site Energies. *J. Chem. Phys.* **2003**, *119* (18), 9809–9817.
(53) López-Estrada, O.; Laguna, H. G.; Barrueta-Flores, C.; Amador-Bedolla, C. Reassessment of the Four-Point Approach to the Electron-Transfer Marcus–Hush Theory. *ACS Omega* **2018**, *3* (2), 2130–2140.
(54) Tummala, N. R.; Zheng, Z.; Aziz, S. G.; Coropceanu, V.; Brédas, J.-L. Static and Dynamic Energetic Disorders in the C60, PC61BM, C70, and PC71BM Fullerenes. *J. Phys. Chem. Lett.* **2015**, *6* (18), 3657–3662.
(55) Faber, C.; Janssen, J. L.; Côté, M.; Runge, E.; Blase, X. Electron-Phonon Coupling in the C60 Fullerene within the Many-Body GW Approach. *Phys. Rev. B* **2011**, *84* (15), 155104.
(56) Le Roux, S.; Petkov, V. ISAACS Interactive Structure Analysis of Amorphous and Crystalline Systems. *J. Appl. Crystallogr.* **2010**, *43* (1), 181–185.
(57) Yokoyama, D. Molecular Orientation in Small-Molecule Organic Light-Emitting Diodes. *J. Mater. Chem.* **2011**, *21* (48), 19187–19202.
(58) Ziener, U.; Lehn, J.-M.; Mourran, A.; Möller, M. Supramolecular Assemblies of a Bis(Terpyridine) Ligand and of Its [2×2] Grid-Type ZnII and CoII Complexes on Highly Ordered Pyrolytic Graphite. *Chem. – A Eur. J.* **2002**, *8* (4), 951–957.
(59) Meier, C.; Ziener, U.; Landfester, K.; Weihrich, P. Weak Hydrogen Bonds as a Structural Motif for Two-Dimensional Assemblies of Oligopyridines on Highly Oriented Pyrolytic Graphite: An STM Investigation. *J. Phys. Chem. B* **2005**, *109* (44), 21015–21027.
(60) Ziener, U. Self-Assembled Nanostructures of Oligopyridine Molecules. *J. Phys. Chem. B* **2008**, *112* (47), 14698–14717.
(61) Meier, C.; Landfester, K.; Ziener, U. Adsorbate−Substrate-Mediated Growth of Oligopyridine Monolayers at the Solid/Liquid Interface. *J. Phys. Chem. C* **2009**, *113* (4), 1507–1514.
(62) Meier, C.; Roos, M.; Künzel, D.; Breitruck, A.; E. Hoster, H.; Landfester, K.; Gross, A.; Jürgen Behm, R.; Ziener, U. Concentration and Coverage Dependent Adlayer Structures: From Two-Dimensional Networks to Rotation in a Bearing. *J. Phys. Chem. C* **2009**, *114* (2), 1268–1277.
(63) van der Spoel, D.; J. van Maaren, P.; Larsson, P.; Tîmneanu, N. Thermodynamics of Hydrogen Bonding in Hydrophilic and Hydrophobic Media. *J. Phys. Chem. B* **2006**, *110* (9), 4393–4398.
(64) Bin, Z.; Liu, Z.; Qiu, Y.; Duan, L. Efficient N-Dopants and Their Roles in Organic Electronics. *Adv. Opt. Mater.* **2018**, *6* (18), 1800536.
(65) Bässler, H. Charge Transport in Disordered Organic Photoconductors a Monte Carlo Simulation Study. *Phys. status solidi* **1993**, *175* (1), 15–56.

Insert Table of Contents artwork here